SYNTHESIS OF NANOSTRUCTURED SOLID SOLUTIONS OF THE FLUORITE AND PEROVSKITE TYPE CRYSTAL STRUCTURE

Snežana Bošković[1], Dejan Djurović[1], Marija Čančarević[1], Branko Matović[1], Zorana Dončević-Mitrović[2], Zoran Popović[2], Matvei Zinkevich[3] ,Fritz Aldinger[3], Milan Vlajić[4], Vladimir Krstić[4], Lj. Živković[5]
[1]*Institut za nuklearne nauke "Vinča", p. pr. 522, 11001 Beograd, Srbija*
[2]*Institut za fiziku, Zemun,*
[3]*Max-Planck Institut, PML, Stuttgart , Germany,*
[4] *Queens University, Kinston, On. Canada,*
[5]*Faculty of Electronic Engineering, University of Niš*

Invited Paper

Abstract – *In this lecture the results on the synthesis of nanosized CeO_2, $CaMnO_3$ and $BaCeO_3$ solid solutions will be presented. Two methods were applied: self propagating room temperature synthesis (SPRT) and the modified glycine/nitrate procedure (MGNP). Solid solutions with rare earth dopants in concentrations ranging from 0-0.25 were synthesized. The reactions forming solid solutions were studied. In addition, the characteristics of prepared nanopowders, phenomena during sintering and the properties of sintered samples are discussed.*

1. INTRODUCTION

Great attention has recently been paid to a development of a new generation of solid oxide fuel cells. The new generation of SOFC should be able to operate at much lower temperatures with rather high efficiency, as compared to currently developed ones. Therefore there is a demand for new materials which will fulfil the necessary conditions for the above said application. In addition, the materials should be less expensive, and produced by application of low cost technologies, including starting powders production. To be able to develop the compositions with high ionic conductivity which is needed for good electrolyte, many problems have to be solved starting with synthesis of starting powders. The major objective of this paper is to present results on highly effective and simple procedures [1, 2, 3, 4] for synthesis of nanopowders that are good candidates for SOFC components. Since CeO_2 is known for its high ionic conductivity at lower temperatures, it is one of the most promising candidates to be used as an electrolyte. Many dopants, such as rare earth cations, show extended solid solubility in ceria lattice along with increasing ionic conductivity of CeO_2. On the other hand, doped Ca-manganites, as well as, Ba-cerates, as a new generation of materials for future SOFC are also very attractive. Many different powders with perovskite type crystal structure-manganites and cerates - were produced, containing cation dopants on A as well as on B sites or both. Sintering tests were performed and these results are discussed, too. In addition, electrical properties for some of the sintered compositions are presented.

2. EXPERIMENTAL

2.1. SPRT - METHOD

Starting reactants used in the experiments were cerium nitrate (Merck), yttrium nitrate (Alfa Aesar), neodymium nitrate (John Mathey) and sodium hydroxide. All used nitrates were in the form of hexahydrates. Amounts of nitrates and NaOH were calculated according to the nominal composition of the solid solutions: CeO_{2-y} $Ce_{0.90}Y_{0.10}O_{2-y}$, $Ce_{0.85}Y_{0.15}O_{2-y}$, $Ce_{0.80}Y_{0.20}O_{2-y}$, $Ce_{0.75}Y_{0.25}O_{2-y}$, $Ce_{0.90}Nd_{0.10}O_{2-y}$, $Ce_{0.85}Nd_{0.15}O_{2-y}$, $Ce_{0.80}Nd_{0.20}O_{2-y}$, $Ce_{0.75}Nd_{0.25}O_{2-y}$, and $Ce_{0.80}Y_{0.10}Nd_{0.10}O_{2-y}$. The chemicals were not milled. Hand-mixing was performed [3] in alumina mortar for 5 – 7 min until the mixture got light brown. After being exposed to air for 3 h, the mixture was suspended in water. Rinsing of $NaNO_3$ was performed in centrifuge - Megafuge 1.0, Heraeus, at 3200 rpm, for 10 min. This procedure was performed three times with distilled water and twice with ethanol. After drying, powder was analysed by applying X-ray diffraction (XRD, Siemens D-5000), scanning electron microscopy (SEM, Zeiss DSM 982 Gemini), Raman spectroscopy (Jobin-Ivon monochromator), and specific surface area measurement (BET). Chemical analysis of dopants concentration was carried out by titration to check the difference between nominal and true compositions of solid solution powders. To follow the reaction path, differential thermal analysis (DTA) and thermogravimetry (TG, Netzsch STA 409) were performed in air atmosphere, at heating and cooling rates of 5°C/min.

2.2 MGNP-METHOD

Starting chemicals used for the synthesis of powders were aminoacteic acid-glycine, (Fischer Scientific, USA), metallic acetates (Mn, Ba) and nitrates (Ce, La, Y, Nd, Gd, Sm), produced by Aldrich, USA. Synthesis was carried out in a stainless steel reactor in which all reactants dissolved in distilled water were added according to previously calculated composition of the final powder. We used nitrates in the form of solutions, and acetates in the as received form [4]. Glycine was also added in the as received form. The reactants were heated on a hot plate up to about 540°C, until the evolution of the smoke terminated. As a result of modifying GNP, the

reaction proceeded very smoothly. Therefore almost no loss in the synthesized powders quantity was observed. The experimentally obtained amount of powder was very close to the theoretically calculated one, 96-99%. For practical reasons it is very important to outline that the quantity of chemicals was designed to synthesize 100g of powder per run (in 30 min), which is according to our knowledge among the largest scale produced by this method so far. Since the evaporation was not intense during the experiment, the amount of powder produced per run can be even larger if the size of reactor would increase. The following powders were synthesized: $CaMnO_3$(CM), $Ca_{0.7}La_{0.3}MnO_3$(CLM), $Ca_{0.9}Y_{0.1}MnO_3$(CYM1), $Ca_{0.8}Y_{0.2}MnO_3$(CYM2), $Ca_{0.7}Y_{0.3}MnO_3$(CYM3), $Ca_{0.7}La_{0.3}Ce_{0.2}Mn_{0.8}O_3$(CLCM), $BaCeO_3$, $BaCe_{0.9}Gd_{0.1}O_3$, $BaCe_{0.85}Gd_{0.15}O_3$, $BaCe_{0.8}Gd_{0.2}O_3$, $BaCe_{0.8}Nd_{0.2}O_3$, $BaCe_{0.8}Sm_{0.2}O_3$. The obtained ashes were afterwards calcined depending on the composition, at temperatures 800-1010°C, for 2- 4 hours.

3. RESULTS AND DISCUSSION

3.1. SPRT- Reaction development

SPRT procedure is based on the self-propagating room temperature reaction [3] between metal nitrates and sodium hydroxide, and in the case of the doped ceria solid solution the reaction can be written as follows:

$$2\,[(1-x)Ce(NO_3)_3.6H_2O + xMe(NO_3)_3.6H_2O] + 6\,NaOH + (½-\delta)\,O_2 \rightarrow 2\,Ce_{1-x}Me_xO_{2-\delta} + 6\,NaNO_3 + 15\,H_2O \quad (1)$$

During heating of the reacting mixture (Fig.1) a sharp peak is observed on DTA curve showing that the reaction is strongly exothermic

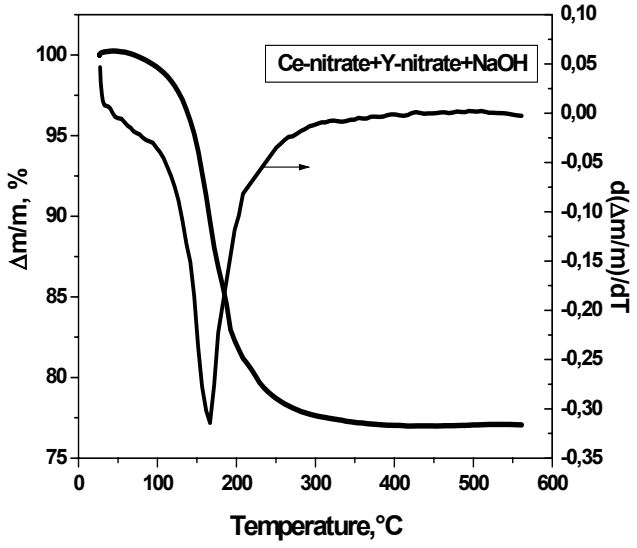

Fig.1. *DTA and DTG curves for cerium nitrate –yttrium nitrate and NaOH mixture.*

At the peak point (about 50 °C) of this exothermic effect, the rate of weight loss starts to increase followed by endothermic effect. The maximum rate at 160 °C (Fig. 1) coincides with the termination of the heat release. This indicates that the reaction is initiated by the rapid, strong heat release, developing easily afterwards.

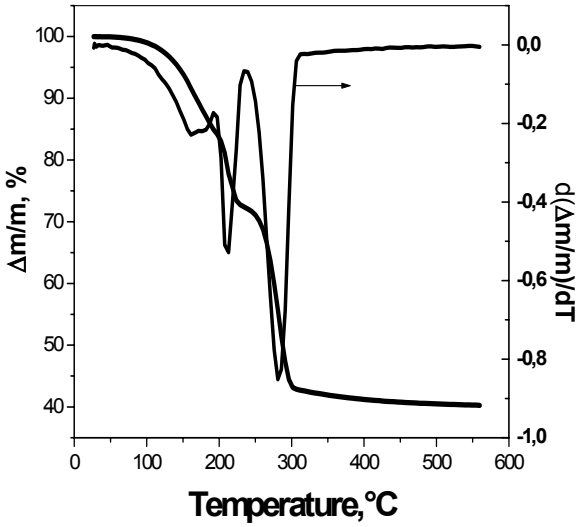

Fig.2 . *TG-DTG curves for pure $Ce(NO_3)_3.6H_2O$.*

However, from Fig.2 it is clear that reaction is taking place via three intermediate steps.The first endothermal effect shows the loss of absorbed water. DTG curve shows three peaks, similar to those on DTA curve[3] which means that each endothermic effect is accompanied by definite mass loss connected with the loss of chemically bound water molecules frim hitrates. Weight loss terminates at 300°C, at which point cerium nitrate hexahydrate was completely converted into ceria after a gradual loss of crystalline water (Fig. 2).

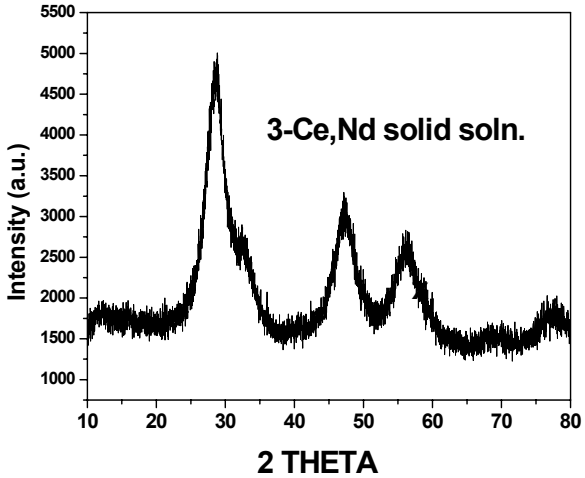

Fig.3. *X-ray pattern of $Ce_{0.90}Nd_{0.10}O_{2-\delta}$ powder.*

Extremely low reaction temperatures indicated that by introducing mechanic energy into the system, reaction would, also be easily initiated. That is why hand mixing was

performed. XRD of final reaction product is given in Fig. 3. This pattern reveled the charactestic peaks of $Ce_{0.90}Nd_{0.10}O_{2-\delta}$. The mentioned reaction steps, however, could be observed only with the non-homogenized sample in which the reaction proceeds at much lower rate compared to homogenized mixture, (Fig.4). To make the reaction steps to be obvious, the two substances $Ce(NO_3)_3.6H_2O$ and NaOH, were brought into contact and just allowed to react for 24 h. In the X-ray pattern of this sample (Fig. 4), the diffraction lines of final reaction products CeO_2 and $NaNO_3$ were detected, along with intermediate reaction products, that are mainly Ce-nitrates with lower number of crystalline water moluecules.

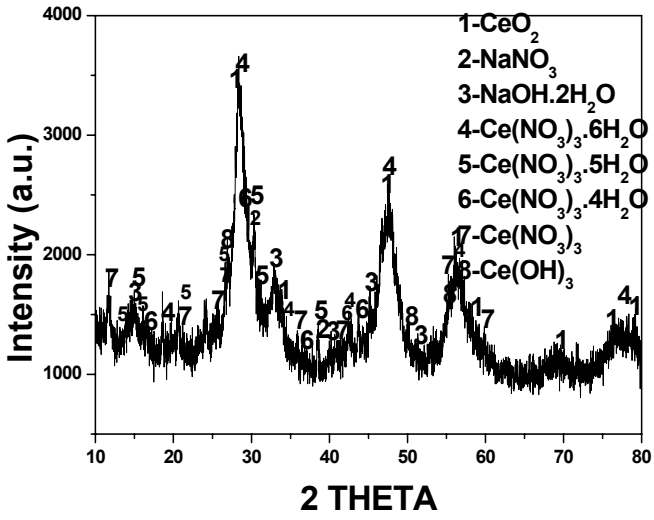

Fig. 4. *X-ray pattern of non homogenized mixture*

These results are in agreement with the ones in Fig. 2. Raman spectroscopy was performed at room temperature to prove the formation of solid solutions. In Fig. 5 Raman spectra of pure CeO_2, and solid solution powders are presented. The solid solutions retain cerium fluorite structure without the Raman modes of pure dopant oxides. The shift to lower energies of the main F_{2g} Raman mode from 465 cm^{-1} (in bulk) to 454 cm^{-1} (CeO_2 sample) and its asymmetrical broadening indicate the strong phonon confinement effect in these nanopowders. In doped samples this mode is red or blue shifted regarding the CeO_2 nanostructured sample, depending on the dopant ionic size. Additional Raman mode at 599 cm^{-1} in pure ceria nanopowder [5, 6] originates from intrinsic oxygen vacancies due to the powder's nonstoichiometry while the appearance of a new Raman feature in doped samples at 454 cm^{-1} is due to the extrinsic O^{2-} vacancies in fluorite structure in order to keep charge neutrality when Ce^{4+} ions are partly replaced with Nd^{3+}(Y^{3+}) ions. From the Raman spectra we concluded that we are not dealing with simple mechanical mixtures of oxides, but with their solid solutions. In addition to Raman spectroscopy results lattice parameters dependence on dopants concentration obey Vegard's law, proving that solid solution were synthesized [1] indeed.

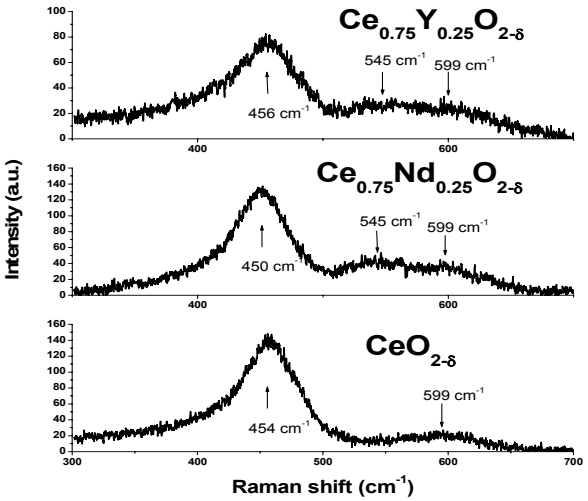

Fig.5. *Raman spectra of pure and doped ceria*.

3.1.1. Powders Properties

Specific surface areas, crystallite size, particle size, true composition and sodium content after washing of the synthesized powders are given in Tabs.1 and 2.

Table 1: *Properties of "as prepared" SPRT powders*

Composition	Crystallite size (nm)	Surface area /m^2/g/	particle size (nm)
CeO_2	4,18	106.9	16
$Ce_{0.90}Y_{0.10}O_{2\ \delta -}$	4,25	103.2	14
$Ce_{0.85}Y_{0,15}O_{2-\delta}$	4,22	137.1	
$Ce_{0.80}Y_{0.20}O_{2-\delta}$	4,99	109.7	
$Ce_{0.75}Y_{0.25}O_{2-\delta}$	5,62	94.0	
$Ce_{0.90}Nd_{0.10}O_{2-\delta}$	4,36	118.4	
$Ce_{0.85}Nd_{0.15}O_{2-\delta}$	4,35	137.6	
$Ce_{0.80}Nd_{0.20}O_{2\ \delta -}$	4,19	141.5	10
$Ce_{0.75}Nd_{0.25}O_{2-\delta}$	4,12	99.6	
$Ce_{0.80}Y_{0.10}Nd_{0.10}O_{2-\delta}$	4,49	110.0	12

Table 2: *Chemical analysis of "as prepared" powders*

Composition	True composition	Na/wt.%/
CeO_2		
$Ce_{0.90}Y_{0.10}O_{2\ \delta -}$	$Ce_{0.904}Y_{0.096}O_{2-\delta}$	0.05
$Ce_{0.85}Y_{0,15}O_{2-\delta}$		
$Ce_{0.80}Y_{0.20}O_{2-\delta}$		
$Ce_{0.75}Y_{0.25}O_{2-\delta}$		
$Ce_{0.90}Nd_{0.10}O_{2-\delta}$	$Ce_{0.914}Nd_{0.086}O_{2-\delta}$	0.07
$Ce_{0.85}Nd_{0.15}O_{2-\delta}$		
$Ce_{0.80}Nd_{0.20}O_{2\ \delta -}$		
$Ce_{0.75}Nd_{0.25}O_{2-\delta}$	$Ce_{0.78}Nd_{0.22}O_{2\ \delta}$	0.005*
$Ce_{0.80}Y_{0.10}Nd_{0.10}O_{2-\delta}$	$Ce_{0.828}Y_{0.085}Nd_{0.087}O_{2-\delta}$	0.008*

*increased number of rinsing runs

Crystallite size was obtained on the basis of XRD data, while the particle size was measured from SEM images (Fig. 6).

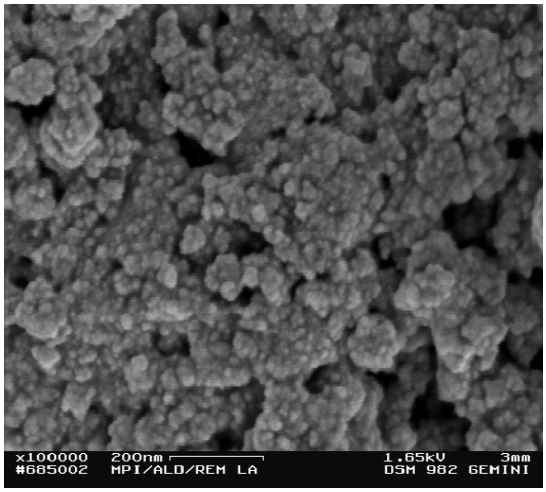

a

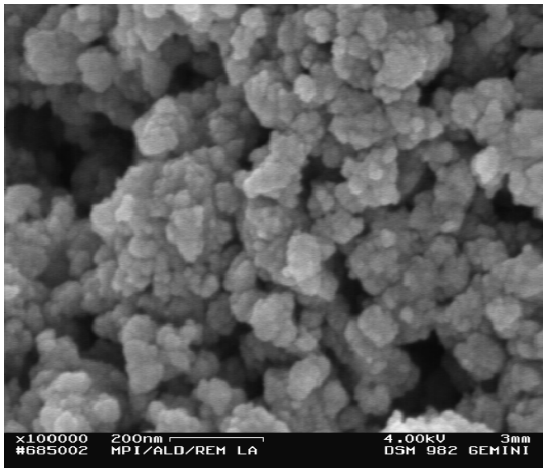

b

Fig.6. *Y doped (a) and Y, Nd co-doped (b) ceria solid solution*

3.2. MGNP- PROCEDURE

Glycine – nitrate process is based on the self-combustion of the glycine and nitrate mixture, according to the reaction that could be described as

$$2\ NH_2CH_2COOH + ME^1(NO_3)_3.6H_2O + ME^2(NO_3)_3.6H_2O] + 2\ O_2 \rightarrow$$

$$ME^1ME^2O_3 + 22\ H_2O\uparrow + 4\ N_2\uparrow + 4\ CO_2\uparrow$$

which spontaneously occurs at about 180°C. Glycine plays in this reaction double role, it acts as a fuel and on the other hand as a complexant. By complexing with present cations their selective precipitation prior to ignition (after the water had been evaporated) is prevented. The reaction is, as mentioned, very intense and needs to be controlled. There are different possibilities to control the reaction rate, and thereby the reaction temperature in order to obtain finer particles and larger specific surface area. We modified [4] the original GNP procedure [2] by replacing partially as discussed above, nitrates by acetates. Acetates are water soluble, and are less expensive compared to nitrates of same purity. To prove the difference between powders obtained by GNP and MGNP we synthesized $CaMnO_3$ by both procedures. X-ray patterns of the two ashes [4] showed as the only difference the fact that $CaMnO_3$ ash obtained by GNP was more crystallized, which was to be expected because of higher temperatures developed during GNP as compared to MGNP. However, better crystallized powder due to faster growth of crystallites resulted in decreasing of specific surface area. By applying this method we managed to produce different powders with more than one dopant cation, of very precise stoichimetry and nanometric particle size. Most of the ashes that are obtained immediately after synthesis were partially amorphous. However, the powders obtained after calcination were all single-phase powders i.e. solid solutions. Peaks related to isolated dopant oxides or secondary phases were not observed. All of them exhibit perovskite type crystal structure. The example in Fig. 7 is given for Y-doped $CaMnO_3$.

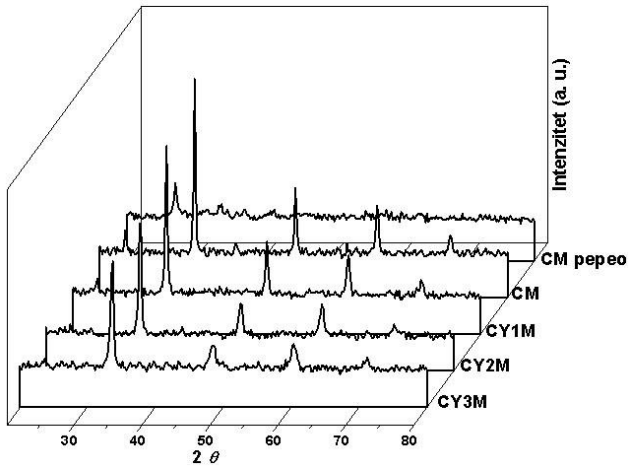

Fig.7. *X-ray patterns of $CaMnO_3$ compositions*

3.2.1 Powders properties

The XRD patterns of all powders looked similar to each other, despite the different amount of dopant. However, a slight difference of peak widths as well the shifting the peaks toward lower angles with increasing dopant amounts were observed. This indicated the existence of solid solution (Fig. 7) with different crystallite size (Table. 3). Microstructure size-strain analysis showed both crystallite size and crystallite strain increase with dopant insertion into perovskite structure. In cerate group of powders (calcined at 1010°C, 4h) specific surface area almost does not change, neither with cation type nor with the dopants concentration, although the concentration of dopants was doubled (samples 8 and 10, Tab. 3). It seems

that with increasing calcination temperature specific surface area decreases drastically, and all other factors influencing specific surface area are masked.

Table 3. *Specific surface area and dopants concentration for MGNP powders*

Nominal composition ($A_{1-x}B_xO_3$)	Surface area (m^2/g)	Dopants content (wt %)	x in $A_{1-x}B_xO_3$
1. $CaMnO_3$	17.7	-	
2. $Ca_{0.7}La_{0.3}MnO_3$	9.9	19.50±0.40	0.245
3. $Ca_{0.9}Y_{0.1}MnO_3$	17.5	6.13±0.12	0.102
4. $Ca_{0.8}Y_{0.2}MnO_3$	16.3	11.30±0.20	0.195
5. $Ca_{0.7}Y_{0.3}MnO_3$	15.6	16.20±0.30	0.288
6. $Ca_{0.7}La_{0.3}Ce_{0.2}Mn_{0.8}O_3$	13.2	La=20.80 ±0.40 Ce=13.50 ±0.30	0.289 0.184
7. $BaCeO_3$	3.6	-	
8. $BaCe_{0.9}Gd_{0.1}O_3$	3.4	4.46±0.06	0.093
9. $BaCe_{0.85}Gd_{0.15}O_3$	3.1	6.51±0.09	0.164
10. $BaCe_{0.8}Gd_{0.2}O_3$	3.5	7.79±0.12	0.180
11. $BaCe_{0.8}Nd_{0.2}O_3$	3.6	7.82±0.12	0.177
12. $BaCe_{0.8}Sm_{0.2}O_3$	3.5	8.86±0.14	0.193

Chemical analysis data (Tab. 3) show excellent agreement between designed and true composition of all synthesized powders.

Lattice parameters were calculated for all the calcined powders. The results are presented in Fig 8 as the dependence of lattice parameters on dopants concentration (x), as well as, (Fig. 9) on the dopants cation radii (Ba^{2+}-1.34 Å, Ce^{4+}-0.920 Å; Gd^{3+}-0.938 Å; Sm^{3+}-0.964 Å; Nd^{3+}-0.995 Å; La^{3+}- 1.016 Å).

In $CaMnO_3$ doped with Y^{3+}, lattice parameters obey Vegard's law as shown in Fig. 8. The same was found for lattice parameter dependence on Gd concentration in Ba-cerates. Data in Figs. 8 and 9 are very important since phase diagrams are not always known, for they prove, too, that single phase powders are obtained in the concentration range investigated. SEM and TEM analyses were performed for manganites and cerates, respectively.

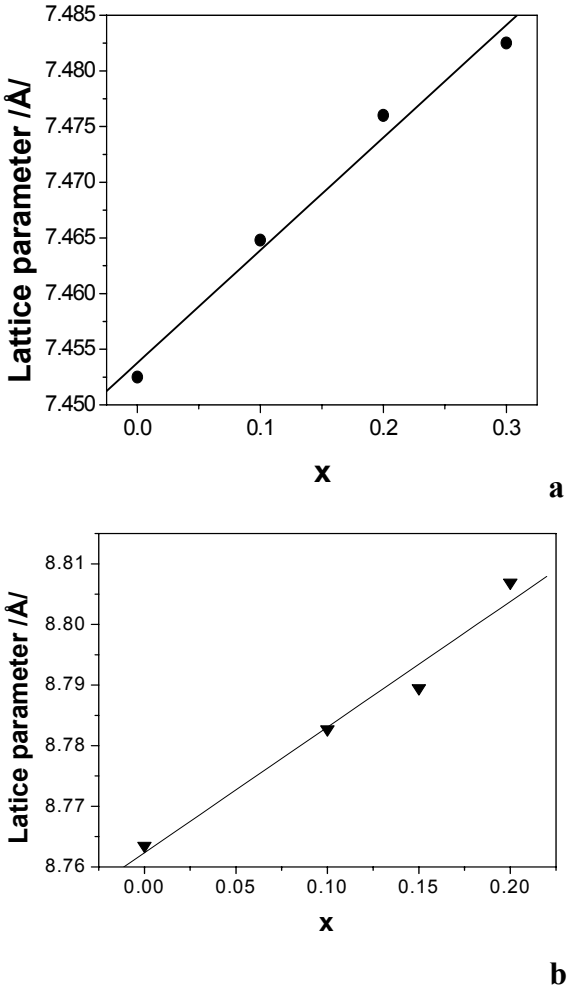

Fig. 8. *Lattice parameters of a. $Ca_{1-x}Y_xMnO_3$ and b. $BaCe_{1-x}Gd_xO_3$ as a function of Y and Gd contents, respectively*

Ca-manganate particles were less than 50 nm in size, which is illustrated in TEM Fig. 9 for $Ca_{0.9}Y_{0.1}MnO_3$ powders obtained after calcining at 800°C, 4 h. Insert picture in the upper right side shows the typical electron diffraction image of the nanocrystal surface which appears disordered, or even amorphous. This matches the XRD results, where short-range order of nanoparticles exhibits diffraction patterns with pronounced X-ray peak broadening. On the other hand, the size of particles of $BaCe_{0.8}Gd_{0.2}O_3$ after calcinations at 1050°C, 4 h, lies in the range of 80-100 nm. It is also obvious form Fig. 9, that cerate particles have already been sintered during calcination, which is in accordance with the results obtained for the specific surface area (Tab. 3), contrary to managanites particles that are calcined as mentioned, at much lower temperature.

3.3. Sintering of Calcium Manganite Powders

Synthesized powders were ball milled in ethanol with zirconia grinding media for 24 hrs and mean particle size was determined by "Horiba" laser particle size analyzer, using ethanol as dispersing fluid.

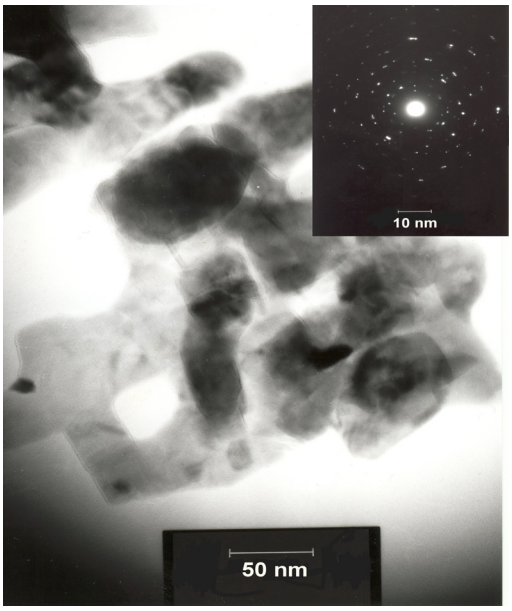

a

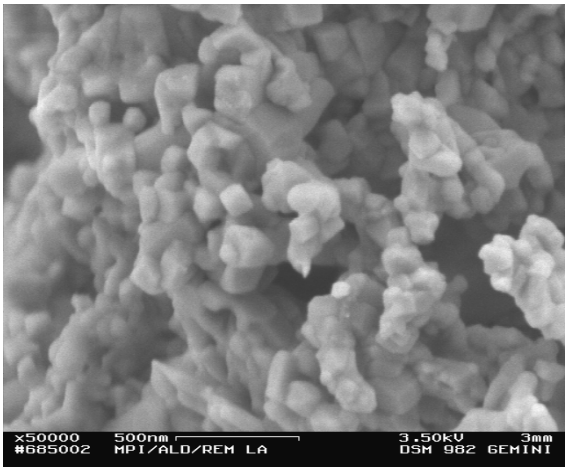

b

Fig. 9 *Microstructures of* $Ca_{0.8}Y_{0.2}MnO_3$ *(TEM) and* $BaCe_{0.9}Gd_{0.1}O_3$ *(SEM) powders*

Powders granulated with 5 wt% of polyethylene glycol as a binder, were compacted by uniaxial pressing under 50 MPa and thereafter cold isostatic pressing under 200 MPa was applied. Burn out of the binder was accomplished under vacuum at 450°C. Sintering was performed in the air in the temperature interval between 1100°C to 1550°C for 2 hrs at a heating rate of 4°C/min up to 1000°C and 2°C/min up to sintering temperature. Cooling rate was 8°C/min. Sintered densities were measured by Archimedes method in hexane. Electrical dc resistance was measured by 4-point method in the range from 25 to 900°C using "Agilent" multimeter with sensitivity of 10 μOhm. Resistance value at any temperature was noted after stabilization.

Green densities of the compositions studied are given in Table 4. Optimum sintering temperatures were determined experimentally for each composition in the range from 1000 – 1550°C. Optimum sintering temperature was considered the one at which highest density was achieved and these data together with sintered densities and the difference between sintered and green densities [7] are summarized in Table 5.

Table 4. *Green densities of selected compositions*

Composition	Green density [g/cm3]	TD [%]
CM $CaMnO_3$	2.2	47.2
CY1M $Ca_{0.9}Y_{0.1}MnO_3$	1,9	40.9
CY2M $Ca_{0.8}Y_{0.2}MnO_3$	1.9	39.7
CY3M $Ca_{0.7}Y_{0.3}MnO_3$	2.0	39.1
CLM $Ca_{0.7}La_{0.3}MnO_3$	2.4	42.6
CLMC $Ca_{0.7}La_{0.3}Ce_{0.2}Mn_{0.8}O_3$	2.2	35.9

Since specific surface areas and particle size do not differ too much, sintered density values indicate that increasing Y concentration enhanced densification of Ca manganite. The density data obtained at 1150°C for all the Y containing solid solutions show clearly that sintered density increases with increasing Y content in the solid solution. However, the La addition affects the increase of the sintering temperature of Ca manganite, especially in the presence of Ce ions whereby the densification degree dropped. In spite of relatively high specific surface area of these samples, sintering temperature turns to be the highest. The influence of dopants concentration on the densification during sintering can be discussed only in the case of Y containing samples.

Namely, with increasing Y^{3+} ions in the lattice of $CaMnO_3$ on A site, cation vacancies are created. For two Y^{3+} ions introduced into the lattice on A site instead of Ca^{2+}, one cation vacancy is formed for charge compensation. Increasing cation vacancy concentration is not relevant for the increased densification degree, since the rate determining step is oxygen diffusion. However, bearing in mind the case when cation vacancies are dominant lattice defects in the bulk, the grain boundary charge is expected to be positive [8] and would be responsible for enhanced oxygen diffusion along the grain boundaries. This assumption implies that the grain boundary diffusion may be the dominant mechanism of mass transport during sintering, causing densification. This may well be accepted in our case, since we are dealing with nanosized powder particles. In this case the fraction of the grain boundaries in the samples being sintered is extremely high. With introducing La^{3+} at A site the same situation as described above, as far as point defects are concerned appears. On the other hand in the case of co-doped sample some free ceria was detected as mentioned,

Table 5. *Sintering Temperatures, Sintered Densities and ds-di parameter*

Nominal Composition	Sintering Temperature [°C]	Sintered Density [g/cm3]	Sintered Density [TD%]	ds-di** [%]
CM $CaMnO_3$	***1250**	**4.54**	**99.1**	
CM $CaMnO_3$	**1150**	**4.06**	**88,6**	**51.6**
CY1M $Ca_{0.9}Y_{0.1}MnO_3$	***1200**	**4.48**	**94.9**	
CY1M $Ca_{0.9}Y_{0.1}MnO_3$	**1150**	**4.38**	**92,8**	
CY2M $Ca_{0.8}Y_{0.2}MnO_3$	***1150**	**4.40**	**91,0**	**51.3**
CY3M $Ca_{0.7}Y_{0.3}MnO_3$	***1150**	**4.84**	**94.5**	**53.1**
CLM $Ca_{0.7}La_{0.3}MnO_3$	***1350**	**5.20**	**94,2**	**55.4**
CLMC $Ca_{0.7}La_{0.3}Ce_{0.2}Mn_{0.8}O_3$	***1450**	**5.29**	**87.4**	

*optimum sintering temperature, ** ds-sintered density, di-green density [TD%]

and the influence of dopants on densification cannot be discussed on the basis of the results obtained.
SEM micrographs of sintered samples are presented in Fig. 10. It can be seen that the densities [7] of undoped and Y doped samples achieved high degree, while in La doped samples considerable fraction of closed porosity can be observed. The pores are located both between and within the grains. In addition, it is obvious, that by doping $CaMnO_3$ grain growth process is largely affected. Both dopants, La and Y, suppress grain growth, which is especially outlined in Y containing samples. On the basis of these results it is obvious that Y cations promote densification, as well as, formation of fine grained microstructures, that is important for the properties, like electrical conductivity, given in Fig. 11.

The effect of doping and the electrical conductivity-temperature behaviour on different $CaMnO_3$ based compositions can be seen in Fig.11. The obtained results clearly show that both La and Y doped compositions, exhibit high electrical conductivity, both at room and high temperature, being in the range from $3.2 \cdot 10^2$ Scm^{-1} and $1.7 \cdot 10^2$ Scm^{-1}. Bearing in mind that for useful SOFC operation the acceptable levels of electrical conductivity for cathode material is $\sigma > 10^2$ Scm^{-1} [5, 9, 10, 11], the electrical conductivity of the obtained perovskite solid solutions $Ca_{0.7}La_{0.3}MnO_3$, $Ca_{0.8}Y_{0.2}MnO_3$ and $Ca_{0.7}Y_{0.3}$ MnO_3 satisfy this requirements.

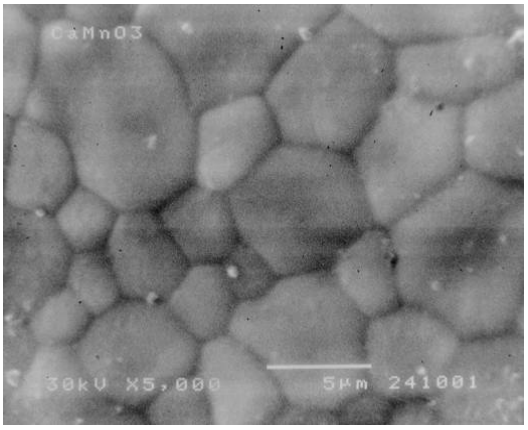

a

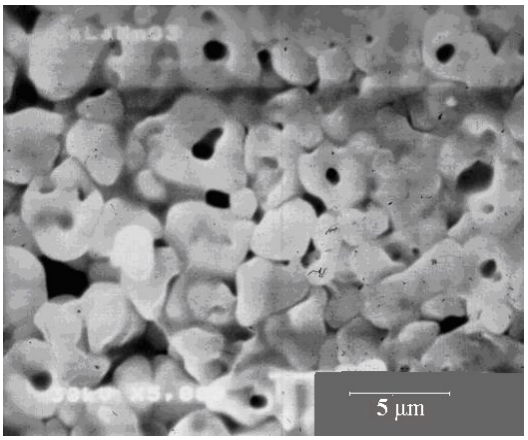

b

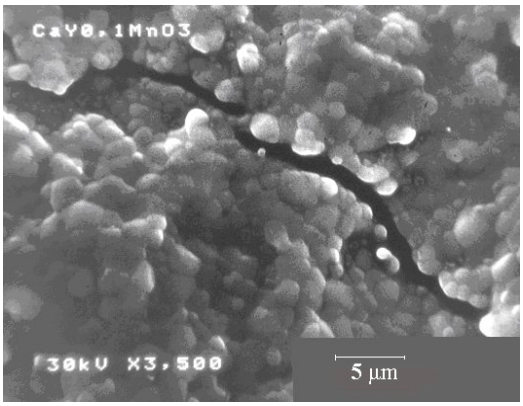

c

Fig.10. *SEM micrographs of sintered pure and doped $CaMnO_3$, a) pure $CaMnO_3$, b) La doped $CaMnO_3$ and c) Y doped $CaMnO_3$ sintered at optimum temperatures*.

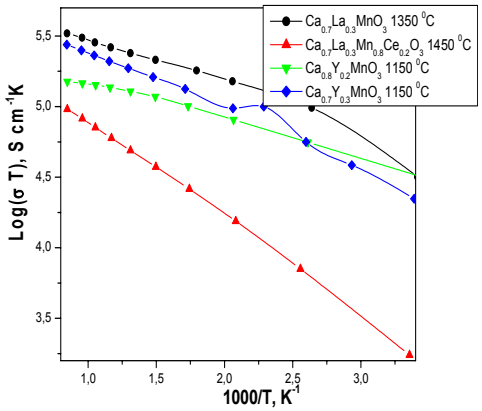

Fig. 11. *Plot Log (σT) vs. 1/T for doped $CaMnO_3$*

4. CONCLUSION

The SPRT reaction proceeds via several intermediate stages due to the stepwise release of crystalline water from nitrate. The reaction steps, however, develop very fast and cannot be observed in the reacting mixture. On the basis of Raman spectroscopy studies it was shown that the solid solutions of $Ce_{1-x}Me_xO_{2-y}$ with one and two dopants can be synthesized by SPRT. It should be emphasized that:

- the reaction starting at room temperature is much less energy consuming in comparison with other methods of powder preparation.
- single phase nanopowders are obtained in a very short time near the room temperature
- chemical composition can be controlled with a good precision
- calcination step is not needed
- simplicity of equipment is advantageous and cannot be neglected.

Glycine nitrate process (GNP) was modified (MGNP) by partial substitution of nitrates for acetates. The combustion process proceeded very smoothly. Powders with perovskite type structure with cation dopants on A as well as on B sites, or both, were synthesized. Loss of powder during synthesis was negligible. The amount of 100 g of powder was produced per run. Very precise stroichiometry was obtained in accordance with tailored composition. Powders were very active, clean, single phase and nanometric in size. It should be pointed out again, that by applying this method

- Large amount of powder can be produced in a very short time
- Single phase nanopowders with high specific surface (among highest published**)** area are obtained
- No intermediate phases were detected
- Instrumentation is very simple
- Very precise control of stoichimetry is possible all over the batch
- The method is flexible of forming complex compositions

Sintering test for manganites showed that full density was achieved at lower sintering temperatures. In creasing Y concentration enhanced densification of manganites, and suppressed grain growth process during sintering. Electrical productivity is highly accepted for SOFC components.

REFERENCES

[1] X. Yu, Feng Li, X. Ye, X. Xin, Ziling Xue, Synthesis of Cerium (IV) Oxide Ultrafine Particles by Solid State Reactions *J.Am.Ceram. Soc*.Vol.83, No.4, 964-66 (2000)

[2] L.A. Chick, L.R. Robertson, G.D. Maupin, J.L. Bates, L.E. Thomas, and G.J. Exarhos, Glycine-nitrate combustion synthesis of oxide ceramic powders, *Materials Letters*, Vol.10, (1999), 6-12

[3] S. Boskovic, D. Djurovic, Z. Dohcevic-Mitrovic, Z. Z. Popovic, M. Zinkevich, F. Aldinger, Self Propagating room temperature szntheis of nanopowders for SOFC. *Journal of Power Sources*, 145, (2005), 237-242

[4] S. B. Bošković, B. Z. Matovic, M. D. Vlajić and Vladimir D. KristićModified Glycine Nitrate Procedure (MGNP) for the Synthesis of SOFC Nanopowders Ceramics International, (2006), Article in Press

[5] Z. D. Dohčević-Mitrović, M. J. Šćepanović, M. U. Grujić-Brojčin, Z. V. Popović, S. B. Bošković, B. M. Matović, M. V. Zinkevich and F. Aldinger The size and strain effects on the Raman spectra of $Ce_{1-x}Nd_xO_{2-\delta}$ ($0 \le x \le 0.25$) nanopowders *Solid State Communications*, 137, (2006), pp. 387-390

[6] Z D Dohcevic-Mitrovic, M.J. Scepanovic, M.U.Grujic-Brojcin, Z.V. Popovic, S.B. Boskovic, B.M. Matovic, M.V. Zinkevich, F. Aldinger $Ce_{1-x}Y(Nd)_xO_{2-\delta}$ nanopowders: potential materials for intermediate temperature SOFCs, Jou*rnal of Physics: Condensed Matter*, 2006, Articles in Press

[7] S. Boskovic, J. Dukic, B. Matovic, Lj. Zivkovic, M. Vlajic, V. Krstic Synthesis, sintering and electrical conductivity of calcium manganite solid solutions, to be published

[8] F.A. Kroeger, *Point Defects in Compounds and Their Role in Diffusion, Sintering and Related Phenomena*, Ed. C.G.Kuczynski, Gordon and Breatch Science Publ.1967, p.57

Acknowledgement

The authors are grateful to Ministry of Science and Environmental protection of Serbia, The Humboldt Foundation, Germany, and National Science and Engineering Council of Canada, for supporting this paper which is a part of ON 142003 project.